Solid Freeform Fabrication 2018: Proceedings of the 29th Annual International Solid Freeform Fabrication Symposium – An Additive Manufacturing Conference
Reviewed Paper

Establishing Property-Performance Relationships through Efficient Thermal Simulation of the Laser-Powder Bed Fusion Process

Mohammad Masoomi, Basil Paudel, Nima Shamsaei, Scott M. Thompson*

Department of Mechanical Engineering, Auburn University, Auburn, AL, 36849

National Center for Additive Manufacturing Excellence (NCAME), Auburn University, AL, 36849

29th Annual International Solid Freeform Fabrication Symposium - An Additive Manufacturing Conference

Abstract

In order to learn how to modify additive manufacturing designs and processes to ensure lab-scale specimens and final components have similar properties, it is important that process-property relationships be established through thermal simulations. In this study, two unique numerical methods for efficiently predicting the thermal history of additively manufactured parts via simulation are presented and validated. These numerical methods make use of an idealized, constant/uniform heat flux which is applied at each new layer and 'bulk-layers' which consist of several layers and allow the use of coarser meshes and longer time steps. To demonstrate and test the numerical methods, simulations are ran for the laser-powder bed fusion (L-PBF) of stainless steel (SS) 17-4 PH parts with different volumes. Simulation results indicate how to modify L-PBF process parameters, specifically time intervals, to better ensure a similar thermal history, temperature, temperature gradient and cooling rate, of different sized/shaped parts.

KEYWORDS: Laser-powder bed fusion, numerical simulation, numerical modeling, temperature gradient, part performance

Introduction

Laser-Powder Bed Fusion (L-PBF) is an additive manufacturing (AM) method that uses a focused laser beam for selectively melting a thin bed of compacted powder material track-by-track and layer-by-layer to produce a solid part, typically within an inert atmosphere purged at a specific flow rate [1]. Due to the high heat flux required for melting powder metal, L-PBF parts experience extremely localized temperature gradients and highly dynamic heating/cooling rates. The single (i.e. sensible) and multi-phase (i.e. latent) heat transfer rates that occur during L-PBF depend on process parameters, such as laser power, laser beam size, and traverse speed. Other design parameters, such as scan patterns, build orientation, powder size, and more, can affect the resultant thermal history of AM parts, as well [2].

Since the thermal response of a part during its AM influences its microstructure, residual stress and defect formation, it is important to predict and model the inherent heat transfer as a

* corresponding author: smthompson@auburn.edu

function of part material type, geometry, location, orientation, operating environment, laser scan strategy, laser power, etc. By understanding these process-property relationships, one gains more control over the AM part/process design for building higher quality parts that meet constraints. These process-property relationships enable end-users to reduce the number of trial-and-error experiments required to learn optimal process/design parameters for a given material.

In-lieu of solving a complex set of governing, partial differential equations for the L-PBF problem, numerical simulation is employed, e.g. finite element methods (FEM) and/or computational fluid dynamics (CFD). The finite element method (FEM) may be used for numerically solving the discretized conservation equations via computational resources. The FEM discretizes the domain into thousands, or millions, of elements in which the conservation equations are applied iteratively using algebraic methods. Modeling and simulation techniques will play a critical role in advancing AM by providing a means to quantify how process variables affect resultant component properties [3]. Through effective process modeling, the underlying transport physics can be better understood and final, AM part production and qualification can be accelerated.

A major challenge in simulating the AM process is developing an efficient model that can produce information and knowledge at the overall scale of the desired part/component and build-process to inform engineering decisions [4,5]. Quantities of interest at the part scale include: distortions that can halt machine operation or place the completed part outside the desired geometric envelope; residual stresses that can create initial conditions detrimental to service-life concerns such as failure and fatigue; and local effective material properties, or at least indicators of where they might significantly deviate from the nominal properties expected from the process. There can be kilometers of laser travel length and thousands of powder layers in a single build, thus presenting a computational challenge. To be useful, part-scale simulations must be executable in a reasonable amount of time while retaining sufficient physical fidelity as to yield trustworthy results. An eventual goal is to have process models that are so efficient they could be included as part of an automated process optimization. Moran et al. [6] used a superposition-based approach to simplify and expedite the simulation process. By modeling a single track and using data from that line and applying it as a line heat source for each track, the simulation time decreased by an order-of-a-magnitude.

To expedite the simulation process and gain the ability to perform simulation on large-scale parts, new techniques are proposed herein. Bundles of layers are combined prior to simulating layer-wise AM in which an effective, uniform heat flux is employed. The goal is to decrease the total number of layers simulated for large-scale parts, thus reducing computational demand and time investment. The methods herein can aid research into AM process/design offsetting to ensure lab-scale specimens and real-life components have similar thermal histories. Numerical results are compared to experimental findings from the literature.

Theory

For modeling the L-PBF process, typically each layer is simulated separately along with a partition/island scheme and scan strategies. A typical part consists of hundreds of layers and thousands of meters of scan paths. In the proposed method, the heat flux applied at the top layer is assumed uniform. The time required to build a rectangular section is then calculated as:

$$t = \frac{m \times l}{w \times v} \tag{1}$$

where l is the length of the rectangular layer, m is the thickness of the part, w is the hatching space, and v is scanning speed. The constant heat flux applied at the top of the layer is calculated as:

$$q'' = \frac{P}{m \times l} \tag{2}$$

where P is laser power. Another method used to facilitate simulations is a method of combining multiple layers together to form a "bulk-layer" – in which the numbers of layers required to model the AM of a part is decreased significantly. Increasing the number of layers in each bulk layer will decrease computational time at the cost of accuracy.

Validation

Tetrahedral meshes were used for the powder bed and were uniformly dispersed, being ~0.05 mm^3 in size (mesh lengths of ~ 0.5 mm). To ensure mesh independent results, simulations were repeated with mesh with lengths of 0.25 mm. No major changes were observed in the simulation results. The numerical model was built using COMSOL® Multiphysics 5.2. Simulations were conducted using the 'Hopper' cluster at the High Performance Computing Center at Auburn University. Each job utilized 80 processors and a total of 128 GB memory. Employed simulation results were validated using data from L-PBF experiments conducted by Dunbar et al. in which a local temperature response was recorded using a thermocouple at the bottom of the substrate [7]. In these experiments, two Ti–6Al–4V parts with geometries of 6.35 x 6.35 x 1.5 mm^3 and 31.8 x 31.8 x 0.24 mm^3 were fabricated. The time interval for both cases was 10 seconds. The substrate size for fabrication of the parts was 89 x 26 x 0.81 mm^3 and 89 x 36.9 x 3.2 mm^3, respectively. The process parameters for the L-PBF process are presented in Table 1.

Table 1. Parameters used for simulating the L-PBF of Ti–6Al–4V parts.

System	EOS M280
Substrate material	Ti–6Al–4V
Powder description	Gas-atomized, air-dried
Powder layer thickness	30 µm
Laser spot diameter	100 µm
Laser power	280 W
Scan speed	1200 mm/s

Two different simulations were conducted to compare the accuracy of each proposed modeling technique. First a constant heat flux was applied to each layer and the process was

continued layer-by-layer until the whole part was simulated (S1). Second, a constant heat flux was applied at the surface of bulk-layers (S2). The temperatures predicted at the bottom of the substrate for S1-S2 are presented in Table 2. The simulation of a 31.8 x 31.8 x 0.24 mm^3 part for S1-S2 took approximately 3 hours and 30 minutes, respectively. The difference between temperature prediction and experimental results for fabrication of the small part was 20 ºC and 35 ºC for S1 and S2, respectively. For the larger part, the temperature difference between the experimental results and the S1 and S2 simulation results was 25 ºC and 35 ºC, respectively.

Table 2. Comparison between experimental results from Dunbar et al. [7] and different simulations conducted of Ti–6Al–4V 6.35 x 6.35 x 1.5 mm^3 part.

No	Experimental result [7]	Simulation #1	Simulation #2
1	105 ºC	125 ºC	140 ºC
2	305 ºC	330 ºC	340 ºC

It may be observed in Fig. 1 that the substrate and powder bed absorb thermal energy from the fabricated parts. Additionally, it is observed from Fig. 2 that by fabricating a larger part and adding more power to the system, the effects of heat accumulation become more marked. Results suggest that modelling each layer separately via an 'effective'/uniform laser heat flux (S1) is more accurate than a bulk layer approach (S2). However, when a constant heat flux is applied at the top of each layer the predicted temperature is higher than the measured temperature. This error could be explained by the fact that heat has less time to diffuse compared to when a local heat flux is modeled. Although individual layer modeling results in more accurate results, the traditional approach requires significantly longer computation times when compared to the proposed techniques.

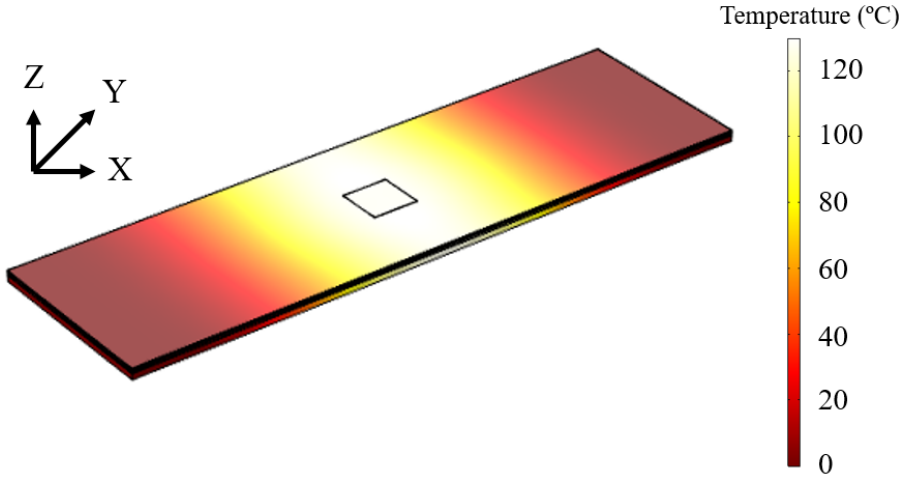

Figure 1. Temperature distribution of Ti–6Al–4V 6.35 x 6.35 x 1.5 mm^3 part immediately after fabrication has finished.

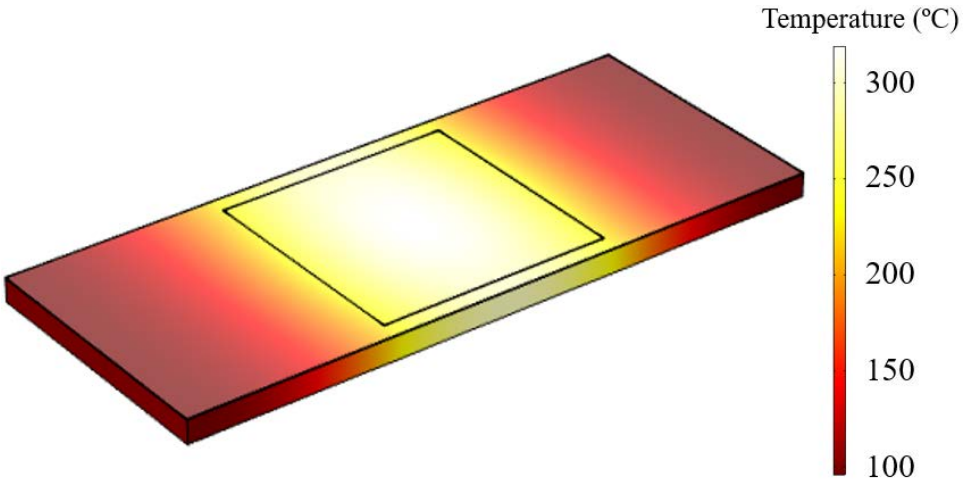

Figure 2. Temperature distribution of Ti–6Al–4V 31.8 x 31.8 x 0.24 mm^3 part immediately after fabrication has finished.

Results

The validated numerical approach was used to investigate the temperature distribution along two different-geometry stainless steel (SS) 17-4 PH parts during L-PBF. One part was a cylinder with two cross-sections, i.e. a 'dog bone', as shown Fig 3 (a). The cylinder had a total length of 84 mm with the top and bottom portions having a diameter of 11 mm and the middle section having a length of 36 mm and a diameter of 7 mm. The other part was a square rod with a cross-section of 11 × 11 mm^2 and thickness of 84 mm, as shown in Fig. 3 (b). Process parameters used for fabrication of these SS 17-4 PH parts are presented in Table 3. The time interval between fabrication of each layer was set at 10 seconds.

Table 3. Parameters used for simulating the L-PBF of a SS 17-4 PH part.

System	EOS M280
Substrate material	SS 17-4 PH
Powder description	Gas-atomized, air-dried
Powder layer thickness	40 µm
Laser spot diameter	100 µm
Laser power	220 W
Scan speed	755 mm/s
Hatching space	110 µm

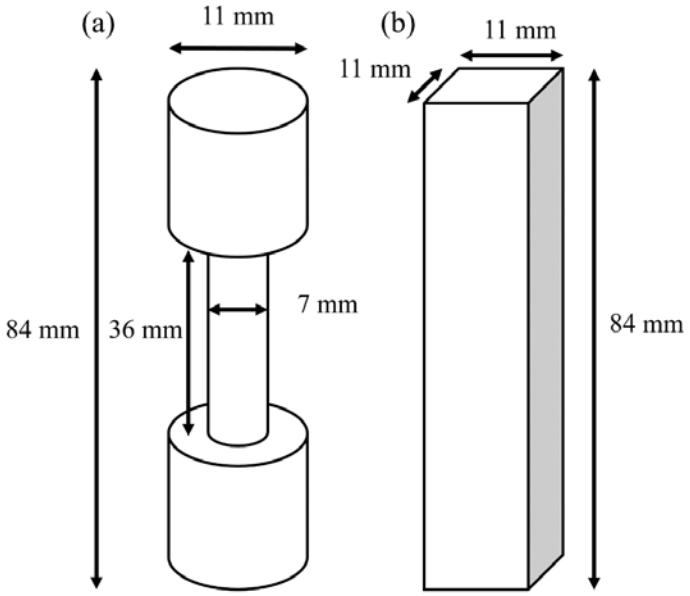

Figure 3. Schematic of L-PBF simulated SS 17-4 PH parts.

The temperature distribution along both parts immediately after fabrication is presented in Fig. 4. It is observed that the temperature along newly-deposited layers is higher relatively to previously-deposited layers. Additionally, it is observed that the cylinder accumulated more heat relative to the square rod. Most of the thermal energy is diffused through fabricated parts. During fabrication of cylinder, the build area is smaller compared to the square rod, thus, heat accumulation becomes more important.

As shown in Fig. 5, the maximum temperature is almost 100 ºC higher on the cylinder relative to the square rod immediately after their L-PBF. This elevated temperature would generally correspond to lower temperature gradients and cooling rates along top portions of the cylinder. It is important to notice that the effects of heat accumulation are more significant along newly-deposited layers and tends to fade away with previously deposited layers. Additionally, it is observed in Fig. 5 that when the build area during fabrication of the cylinder changes, the temperature distribution will significantly be affected. Smaller build area translates to higher heat accumulation.

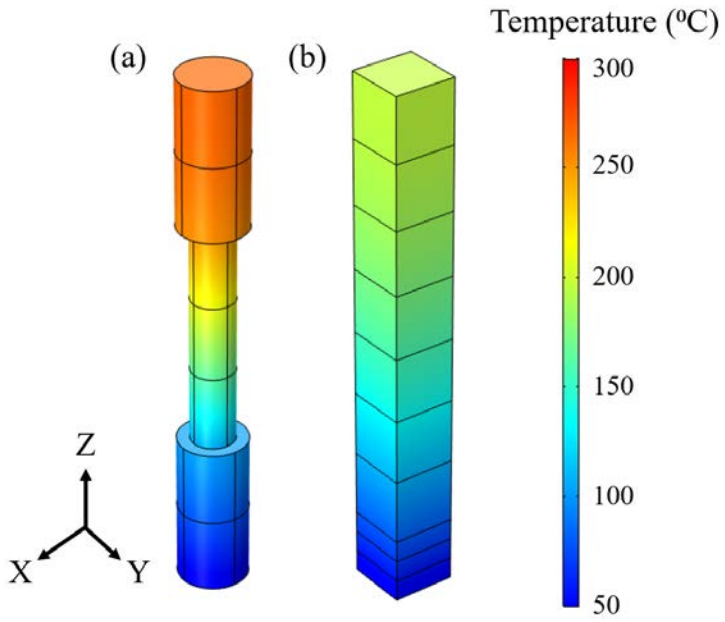

Figure 4. Temperature distribution of (a) cylinder and (b) square rod immediately after L-PBF.

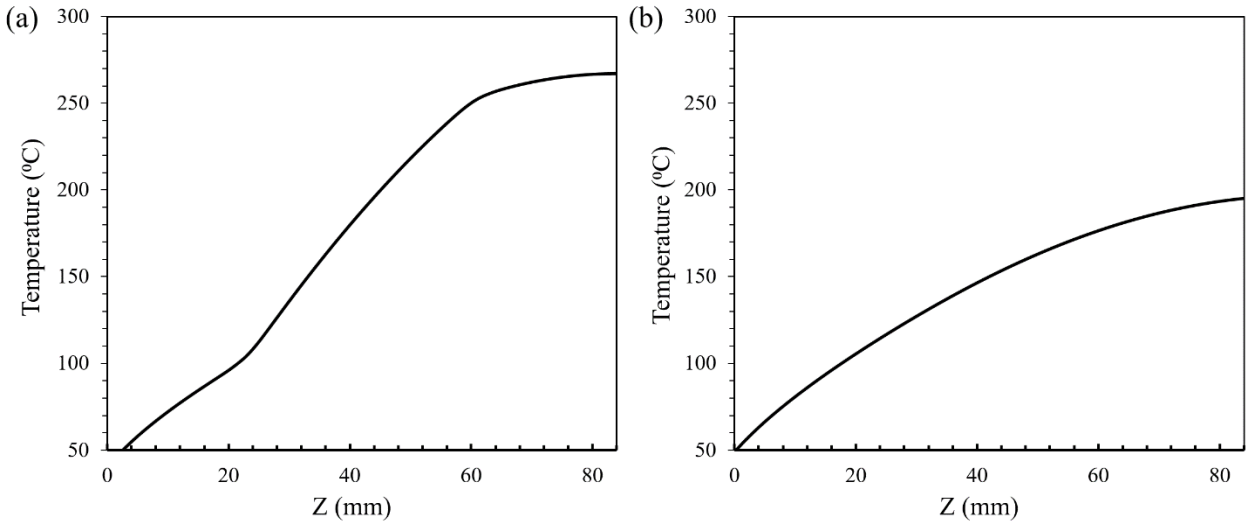

Figure 5. Height-wise (Z) temperature distribution along centerline of (a) cylinder and (b) square rod immediately after their L-PBF.

The different thermal responses shown in Figs. 4-5 indicate that, in general, different-sized/shaped specimens (e.g. cylinder and square rod) will have different microstructural and mechanical properties. In order to fabricate different-sized/shaped parts with similar mechanical properties, which would be important when transitioning from witness/test specimens to full-scale components, it is essential to fabricate parts with the same thermal response, i.e. local cooling rates, absolute temperatures, temperature gradients, etc. In order to achieve this, process parameters must be altered. A simple parameter to control/alter, and one employed herein, is the time interval between layers of fabrication. To demonstrate this, the layer-to-layer time interval the cylinder part was increased from 10 seconds to 15 seconds. It is observed from Fig. 6 and Fig.

7 that, in this case, the thermal response of the cylinder and square rod become much closer to each other.

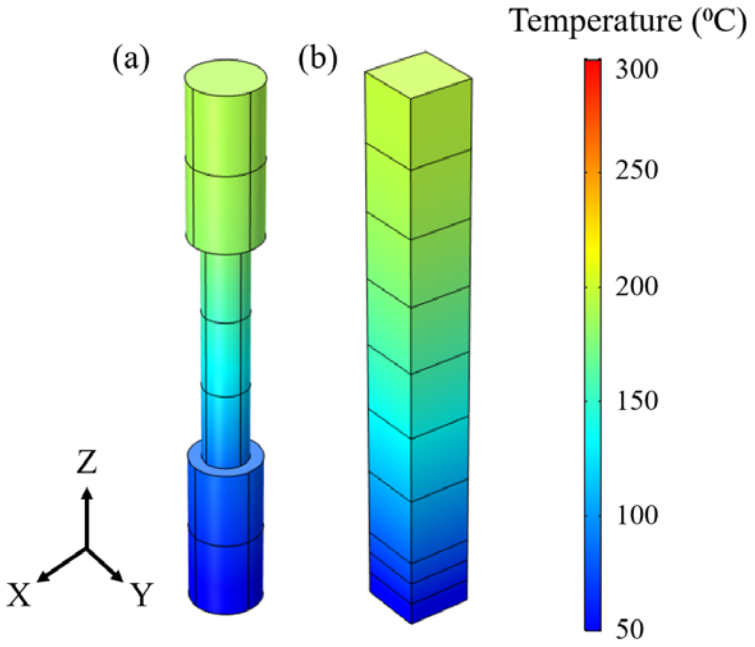

Figure 6. Temperature distribution of fabricated (a) cylinder and (b) square rod after fabrication of the parts.

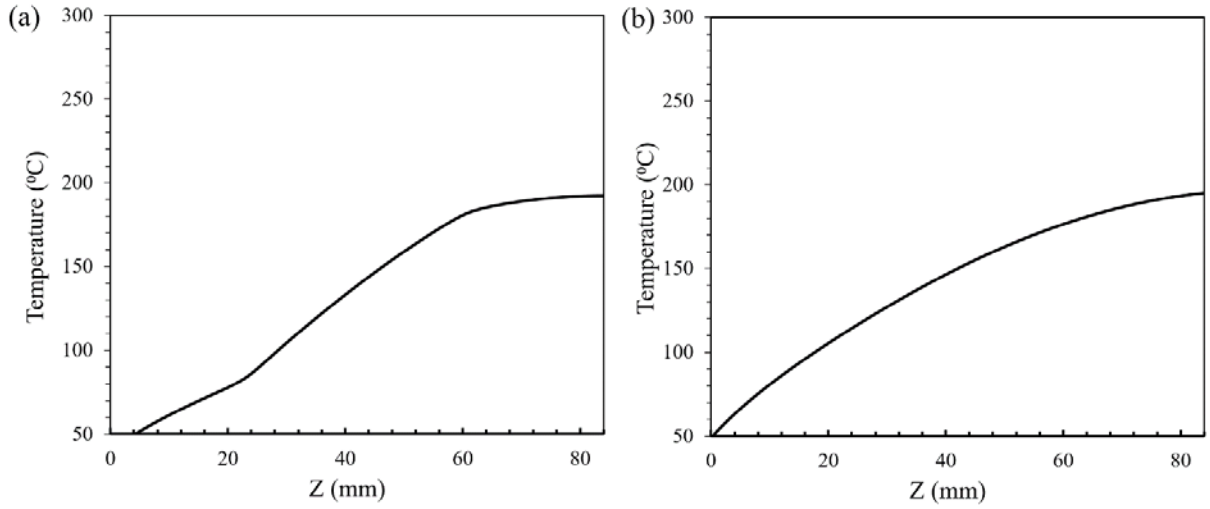

Figure 7. Temperature distribution of (a) cylinder and (b) square rod along the main axis after fabrication of last layer.

Conclusions

In this study, two new techniques were investigated to more efficiently simulate the temperature distribution of part-scale specimens. The techniques were then used to simulate the

thermal response of part-scale specimens. The unique temperature response of different-sized/shaped specimens was demonstrated, and its circumvention shown by increasing the layer-to-layer time interval of the smaller volume part. In general, such an approach can result in parts of almost similar temperature response independent of geometry or build orientation. Major findings of this study are summarized below:

1. By applying constant and uniform heat flux, it is possible to accurately predict heat accumulation during fabrication of the parts efficiently.
2. Bundling layers together prior to simulation will significantly decrease computation times, while only slightly increasing error.
3. Parts with smaller build areas are more likely to experience effects of heat accumulation.
4. Increasing the time interval will decrease effects of heat accumulation.

There continues to be challenges in establishing process-structure-property-performance relationships for AM parts. One may adjust laser power and scan speed during fabrication to achieve target thermal response; however, changing these parameters may affect pore formation in the parts which in turn affects their mechanical response.

Acknowledgment

This work was partially supported by the National Science Foundation under Grant #1657195, and the National Aeronautics Space Administration (NASA) Grant #80MSFC17M0023.

References

[1] M. Masoomi, S.M. Thompson, N. Shamsaei, J. Pegues, Effects of shielding gas flow on heat transfer during laser-powder bed fusion of Ti-6Al-4V, Addit. Manuf. (2018).

[2] M. Masoomi, S.M. Thompson, N. Shamsaei, Laser powder bed fusion of Ti-6Al-4V parts: Thermal modeling and mechanical implications, Int. J. Mach. Tools Manuf. 118–119 (2017) 73–90. doi:10.1016/j.ijmachtools.2017.04.007.

[3] J. Gockel, J. Beuth, K. Taminger, Integrated control of solidification microstructure and melt pool dimensions in electron beam wire feed additive manufacturing of Ti-6Al-4V, Addit. Manuf. 1–4 (2014) 119–126. doi:10.1016/J.ADDMA.2014.09.004.

[4] R. Martukanitz, P. Michaleris, T. Palmer, T. DebRoy, Z.-K. Liu, R. Otis, T.W. Heo, L.-Q. Chen, Toward an integrated computational system for describing the additive manufacturing process for metallic materials, Addit. Manuf. 1–4 (2014) 52–63. doi:10.1016/J.ADDMA.2014.09.002.

[5] T.M. Rodgers, J.D. Madison, V. Tikare, M.C. Maguire, Predicting Mesoscale Microstructural Evolution in Electron Beam Welding, JOM. 68 (2016) 1419–1426. doi:10.1007/s11837-016-1863-8.

[6] T.P. Moran, P. Li, D.H. Warner, N. Phan, Utility of Superposition-Based Finite Element

Approach for Part-Scale Thermal Simulation in Additive Manufacturing, Addit. Manuf. (2018). doi:10.1016/j.addma.2018.02.015.

[7] A.J. Dunbar, E.R. Denlinger, M.F. Gouge, T.W. Simpson, P. Michaleris, Comparisons of laser powder bed fusion additive manufacturing builds through experimental in situ distortion and temperature measurements, Addit. Manuf. 15 (2017) 57–65. doi:10.1016/J.ADDMA.2017.03.003.